Radiation chemical yields for the losses of typical functional groups in PADC films for high energy protons registered as unetchable tracks

Kusumoto, Tamon ; Mori, Yutaka ; Kanasaki, Masato ; Ikenaga, Ryunosuke ; Oda, Keiji ; Kodaira, Satoshi ; Kitamura, Hisashi ; Barillon, Remi ;…

(Citation)
Radiation Measurements,87:35-42

(Issue Date)
2016-04

(Resource Type)
journal article

(Version)
Accepted Manuscript

(URL)
https://hdl.handle.net/20.500.14094/90005201

Radiation chemical yields for the losses of typical functional groups in PADC films for high energy protons registered as unetchable tracks

Tamon Kusumoto[a], Yutaka Mori[b], Masato Kanasaki[a], Ryunosuke Ikenaga[a], Keiji Oda[a], Satoshi Kodaira[c], Hisashi Kitamura[c], Rémi Barillon[d], Tomoya Yamauchi*[a]

[a] *Graduate School of Maritime Sciences, Kobe University, 5-1-1 Fukaeminami-machi, Higashinada-ku, 658-0022 Kobe, Japan*

[b] *Center for Supports to Research and Education Activities, Kobe University, 1-1 Rokkodai-cho, Nada-ku, 657-8501 Kobe, Japan*

[c] *National Institute of Radiological Sciences, 4-9-1 Anagawa, Inage-ku, 263-8555 Chiba, Japan*

[d]*Institute Pluridisiplinaire Hubert Curien, 23 rue du Loess, 67037 Strasbourg Cedex 2, France*

A series of FT-IR spectrometric studies has been performed to understand the latent track structure in poly(allyl diglycol carbonate), PADC, which were exposed to proton beams with energies of 20, 30 and 70 MeV. These energies are too high to register etchable tracks in PADC. Chemical damage parameters, such as damage density, effective track core radius and radiation chemical yields, for losses of ether bond, carbonate ester bond and CH groups in PADC are evaluated as a function of the stopping power, which were compared to the previous results for 5.7 MeV proton and heavy ions, between He and Xe. Graphs of the chemical damage parameters are given at the wide stopping powers ranging from 1 to 12,000 keV/μm. The decreasing behaviors of the ether and carbonate ester bonds are on the almost identical trends with those of the heavy ions. On the contrary to this, the reducing behavior of CH groups is similar to that of the gamma rays. Different dependence of the chemical damage parameters for the loss of CH groups is found on the stopping powers between the both sides of the detection threshold as an etched track detector.

Keyword : PADC, Protons, Heavy ions, G value

*Corresponding author

Phone: +81-78-431-6307

Fax: +81-78-431-6355

e-mail: yamauchi@maritime.kobe-u.ac.jp (Tomoya Yamauchi)

1. Introduction

Almost 40 years have been passed since the discovery of Poly(allyl diglycol carbonate), PADC, as the most sensitive Etched Track Detector, (Cartwright et al., 1978). Because of the excellent track registration property of PADC, it has been commonly utilized in various branches of science and technology such as neutron dosimetry (Oda et al., 2005), space radiation dosimetry (Doke et al., 1995; Benton et al., 2002), radon detections (Font, 2009), inertial nuclear fusion experiments (Zylstra et al.,2012) and intense laser driven ion acceleration experiments (Fukuda et al., 2009; Nishiuchi et al., 2015). While various application fields spread out, there remain some unsolved aspects of the latent track structure and its formation processes in PADC, which should be so helpful to develop more sensitive track detectors (Yamauchi, 2003).

In this decade, we have been conducting a series of FT-IR spectrometric studies on PADC exposed to gamma rays, protons and heavy ions, in order to understand the modified structure along nuclear tracks. Decreasing behaviors of ether and carbonate ester bonds in PADC have been examined, evaluating the three chemical damage parameters, namely, damage density, which is the number of losses of considered functional groups per unit distance of tracks, effective track core radius, in which the considered chemical groups are lost, and the radiation chemical yield, G value, for each functional group, as a function of the stopping power for protons and heavy ions, as well as gamma rays (Mori et al., 2009, 2011, 2012, 2013; Yamauchi et al., 2008a&b). An exceptional feature of PADC is that the G values for the losses of these bonds are higher at the lower stopping power in each ion. The stopping power cannot be a universal parameter to describe the chemical damage parameters, for instance, clearly greater G values were found for semi-relativistic heavier ions at the same stopping powers (Mori et al., 2012). In our recent study, the losing behavior of CH groups, which is sandwiched by the more radio-sensitive parts of the ether and carbonate ester bonds, was examined, as well as the formation process of OH groups that are the new ending points generated by the irradiation, were investigated quantitatively (Kusumoto et al., 2015). The ratio of the amount of OH groups to the damage density of ether has been also determined. This kind of studies are inevitable for us to develop a new radiation chemical model in PADC, in which the radial dose model is mixed with a simple radio-oxidation kinetic to simulate the G values for ether and carbonate ester bond scissions (Barillon et al., 2015). As described above, our studies have covered a wide range in the stopping power from 10 to 12,000 keV/μm, but these are not enough to understand the latent track structure to know what makes it as etchable one. We need to obtain the decreasing behaviors of these groups in PADC

especially for high energy protons what can never produce etchable tracks, as like as classical radiation of gamma rays. Such information is useful to invite the radial dose theory smoothly to the traditional kinetic model.

We have investigated not only on PADC but also on Poly(ethylene terephthalate), PET and bisphenol A polycarbonate, PC, at the stopping powers between 10 and 12,000 keV/μm. A clear step was found on the effective track core radius and G value for the loss of carbonyl in PET at 300 keV/μm, between He and C ions at the energies below 6 MeV/n, which corresponds to the detection threshold (Yamauchi et al., 2012). The track core size said that the two adjacent C-O bonds between the ethylene groups and ester should be broken inside the track in the radial direction when the latent track is etchable. On the one hand, the G values for the loss of carbonyl in PC are almost independent on the stopping powers (Yamauchi et al., 2010). The G values for the losses of phenyl-ring and methyl groups, which arranged between the two carbonate ester bonds, increased rapidly around 100 keV/μm. It happened between protons and He ions with the energies below 6 MeV/n, which also corresponds to the detection threshold. The breaking of more than two neighboring carbonate ester bonds should be key-phenomena producing the latent tracks, which were developed by following chemical etching in PC. We must find the unique feature of the etchable tracks in PADC from a viewpoint of the chemical damage parameters, as like as PET and PC.

In present study, we extend the examined region of the stopping powers starting from 1 keV/μm and determined the chemical damage parameters for loss of ether bonds, carbonate ester bonds and CH groups. It makes possible for us to compare the decreasing behaviors of these bonds in the both side of the detection threshold. Comparisons are also carried out between the results for high energy protons and that for heavy ions previously obtained.

2. Experimental

A repeat unit of PADC is given in Fig. 1., which has an ether bond in the center and two carbonate ester bonds in symmetrical positions. Each repeat unit combines to polyethylene-like polymer chains at both ends. The molecular formula of PADC is $C_{12}H_{18}O_7$ and the length of the repeat unit is about 2 nm. In the present study, BARYOTRAK with a nominal thickness of 100 μm (Fukuvi Chemical Industry Co., Ltd., Japan) were used as starting materials to obtain the sample of PADC films in a size of 2.5 × 2.5 cm^2, which was made from purified monomers. In order to obtain unsaturated IR spectra, we have reduced the thickness to below 3 μm by chemical etching in KOH

solution. The detail of thinning process has been described elsewhere (Yamauchi et al., 2008b).

Proton irradiations with energies of 20, 30 and 70 MeV were performed in air at the C-8 port of the AVF-930 cyclotron equipped in the National Institute of Radiological Sciences, NIRS, Japan (Kanazawa et al., 2010). The flux was determined using the ionizing chamber during all exposures. The maximum fluence was 7.1×10^{13} ions/cm^2. The beam profile was measured by Gafchromic EBT3 films (Ashland Inc.) prior to each exposure. Beam profile was plane at least within 4 cm in the center which guarantees uniform conditions on the film exposures. In addition to this, the irradiation with 83 MeV Ne ions was made in air at the port of the medium energy irradiation room of Heavy Ion Medical Accelerator in Chiba, HIMAC, NIRS, Japan. The experimental details were given in the previous studies (Mori et al., 2011, 2012). In the followings, the datum of the Ne ions was treated as in the same category with the previously reported values for heavy ions.

FT-IR measurements were performed before and after the irradiation using FT/IR-6100S (JASCO, Japan), the entire system of which can be evacuated, including the interferometer, photon-detector and sample room, during the measurements. This made it possible to avoid rigidly the influence of carbon dioxide and water in air.

3. Results and Discussion

4.1. Chemical damage parameters

FT-IR spectroscopy has an advantage that one can derive quantitative information on each chemical bond composing the polymer networks. Therefore it has been applied to examine irradiation effects on various kinds of polymers (Balanzat et al., 1995; Barillon and Yamauchi, 2003; Dehaye et al., 2003). It has an advantage that one can derive quantitative information on each chemical bond composes the polymer networks. Assignments of absorption peaks in the IR spectra of PADC were given in the literatures (Durraud et al., 1993; Gagnadre et al., 1993; Lounis-Mokrani et al., 2003).

As shown in Fig. 2., the relative absorbance of ether bonds, carbonate ester bonds and CH groups decreases linearly with increasing the fluence of 70 MeV protons as a function of fluence, F, in a unit of ions/cm^2. The relative absorbance, A/A_0, is defined as the ratio of the net absorbance of the considered bond after the exposure, A, to that of the original one, A_0. Since the thickness of each film was not altered by the exposure, the Beer-Lambert law allows us to assume that the relative absorbance is equal to the survival fraction, N/N_0, which is the ratio of the number density of the considered chemical bond,

N, to that of the original, N_0. That is, $A/A_0=N/N_0$. For all examined energies, simple experimental formulas were attained in the form of as the following,

$$A/A_0 = 1-\sigma_i F, \tag{1}$$

where σ_i is an experimentally determined constant in a unit of cm^2 and F is fluence in ions/ cm^2. The value of σ_i corresponds to the slope of each fitting line in Fig. 2., which means the removal cross section for each track, under the combinations of kinds of functional group, incident ions and the energy. The evaluated removal cross sections are summarized with statistical deviations in Table 1, as well as the incident energies and the stopping powers. The listed values of the stopping powers are averaged ones in each film calculated by SRIM code (Ziegler, 2004).

Starting with σ_i, we derived the following three chemical damage parameters, damage density, effective track core radius and the radiation chemical yield (G value). The damage density, L_i, is the amount of loss of considered functional groups per unit distance of the track and it was obtained as a product of σ_i and N_0.

$$L_i = \sigma_i \cdot N_0. \tag{2}$$

The effective track core radius, r_i, is a radial distance from the ion trajectory in which all considered bonds should be lost when the corresponding scissions were occurred in the order of the distance from the track center. It was calculated using the following relation:

$$r_i = \sqrt{\sigma_i/\pi}. \tag{3}$$

In the present experimental condition, the size of beam spot is adequately larger than the radial range of secondary electrons. Then the energy deposition progressed uniformly in spatial. These radiations chemical yield was attained as the ratio of the damage density to the stopping power, as in the following relation:

$$G\ value = \frac{\sigma_i N_0}{\left(\overline{-dE/dx}\right)}, \tag{4}$$

where $\left(\overline{-dE/dx}\right)$ is the average stopping power in each PADC film.

When the G value was constant for the stopping power, the damage density is proportional to the stopping power. Because the effective track core radius is proportional to the square root of the damage density, the core radius will be proportional to the square root of the stopping power provided that the G value is independent to the stopping power. This relation among three chemical damage parameters are useful in the following discussion.

4.2. Scissions of ether bonds

Fig. 3. shows the damage density for loss of ether bonds as a function of the stopping power. The present results for protons with energies of 20, 30 and 70 MeV are plotted as solid square symbols, as well as the previously reported values as open symbols for 5.7 MeV proton and heavy ions whose incident energies were less than 6 MeV/n (Mori et al., 2011). As shown in this figure, the damage density has different dependence on the stopping power between the two regions divided at around 800 keV/μm. The first region with the relatively lower stopping powers contains the values for the protons, He and C ions. It is noteworthy that the present results from high energy protons are on the almost identical trend with He and C ions, as well as 5.7 MeV proton. The second region with the higher stopping powers consists of values for Ne, Ar, Fe, Kr and Xe ions. Using the least square fitting, the following two empirical formulas in the type of power functions against the stopping power were derived, which are also illustrated in Fig. 3. The damage density was expressed as,

$$L_{ether} = 390(-dE/dx)^{0.67}, \quad (5)$$

for the first region and as,

$$L_{ether} = 11.2(-dE/dx)^{1.22}, \quad (6)$$

for the second region with the stopping power, where L_{ether} is in a unit of scissions/μm and the stopping power is in keV/μm.

The effective track core radius for loss of ether bonds as a function of the stopping power is shown in Fig. 4. The present results are plotted as solid square symbols and the previously reported values are given in open symbols (Mori et al., 2011). The present results for high energy protons located well on the extrapolated line from the previous results. The segments of fitted lines were attained for each region as,

$$r_{ether} = 0.19(-dE/dx)^{0.35}, \quad (7)$$

for the first region and as,

$$r_{ether} = 0.04(-dE/dx)^{0.59}, \quad (8)$$

for the second region, where r_{ether} is in a unit of nm and the stopping power is in keV/μm. These formulas were improved from that of the previous study (Mori et al., 2011). In the first, we gave the different formulas for each region. Secondary, the datum for 20 MeV He ions was added in the first region (Mori et al., 2012), as well as that for the 83 MeV Ne ions in the second region.

The core radius is about 2 nm at the boundary of 800 keV/μm, which is equivalent to the length of the repeat unit. In the previous paper, we pointed out that most of the damage in tracks of proton and He ion will be formed within a single repeat unit in the radial direction, while the damage of heavy ion tracks such as Kr or Xe ions will cover more than two neighboring repeat units (Mori et al., 2011). The observed bending on the trends of the damage density and the effective core radius could be related to the radial size of the tracks. The damage along proton tracks with high energies should be formed within the single repeat units in the radial direction. We discuss this point in the following section in detail.

4.3. Scissions of carbonate ester bonds

Figs. 5. and 6. show the damage density and effective track core radius, respectively, for loss of carbonate ester bonds, respectively, as a function of the stopping power. The present results for high energy protons are plotted as solid square symbols, as well as the previously reported values for 5.7 MeV proton and indicating heavy ions (Mori et al., 2011, 2012). As like as those for the ether bonds, it is obvious that there exist the two regions with different dependence on the stopping power for the both parameters, at which divided at around 800 keV/μm, for the both chemical damage parameters. The present results from high energy protons are on the almost identical trend with He and C ions, as well as 5.7 MeV proton, in the both graphs. Using the least square fitting, the following empirical formulas in the type of power functions against the stopping power were derived, which are also indicated in Figs. 5. and 6. The damage density was expressed as,

$$L_{C=O} = 320(-dE/dx)^{0.68}, \quad (9)$$

for the first region with the lower stopping power, and as,

$$L_{C=O} = 8.49(-dE/dx)^{1.25}, \quad (10)$$

for the second region, where $L_{C=O}$ is in a unit of scissions/μm and the stopping power is in keV/μm. The fitted lines for the effective track core radius were also attained for each region as,

$$r_{C=O} = 0.14(-dE/dx)^{0.35} \quad (11)$$

for the first region and as,

$$r_{C=O} = 0.03(-dE/dx)^{0.60}, \quad (12)$$

for the second region, where $r_{C=O}$ is in a unit of nm and the stopping power is in keV/μm. These formulas were also improved from those in the previous study (Mori et al., 2011).

The bending on the trends of damage density and track core radius was observed at the same stopping power of 800 keV/μm to those for the ether bonds, implying association between the scissions of ether and carbonate ester bonds. The damage of the carbonate ester bonds along high energy proton tracks should be also formed within the single repeat units.

4.4. Scissions of CH groups

The damage density for loss of CH groups is shown in Fig. 7., as a function of the stopping power. The three square symbols indicate the present results and the previous results are indicated with open symbols (Kusumoto et al., 2015). It is obvious that the dependence of the present results is fairly different from that of the heavy ions, indicating the clear gap between the protons and heavy ions. The data of 5.7 MeV protons locates between the two line segments, closer to those of high energy protons. The experimental formulas for protons was obtained by the least square fitting, excluding the 5.7 MeV proton, as,

$$L_{CH} = 1780\left(-dE/dx\right)^{1.08}, \tag{13}$$

where damage density, L_{CH}, is in scissions/μm and the stopping power is in keV/μm. The exponent is so close to one. This means that the radiation chemical yield will be almost independent of the stopping power, as discussed in the followings. For heavy ions, it is not normal to divide the plots in two different regions, unlike the ether and carbonate ester bonds. The following formula was derived for heavy ions between He and Xe ions, like as,

$$L_{CH} = 210\left(-dE/dx\right)^{1.12}, \tag{14}$$

where damage density, L_{CH}, is in scissions/μm and stopping power is in keV/μm.

Fig. 8. shows the effective track core radius for loss of CH groups as a function of the stopping power, indicating the gap between the present results for protons and those for other heavy ions, again. The experimental formulas were attained as,

$$r_{CH} = 0.11\left(-dE/dx\right)^{0.47}, \tag{15}$$

for the high energy protons and as,

$$r_{CH} = 0.03\left(-dE/dx\right)^{0.59}. \tag{16}$$

for the heavy ions, where the effective track core radius, r_{CH}, is in nm and the stopping power is in keV/μm.

The detection threshold of PADC as an etched track detector for protons is 2.7 MeV in the energy and 17 keV/μm in the stopping power (Hassan et al., 2013; Kodaira et al., 2013). As indicated as the arrows in Figs. 7. and 8., the detection threshold locates within the gap. The observed gap should relate to the different structure of tracks in the both sides of the detection threshold. The effective track core radius is 0.3 nm at the gap, in which the damage along proton tracks should be within single repeat units.

4.5. Radiation chemical yields

Figs. 9. and 10. show radiation chemical yields for losses of ether bond and carbonate ester bond, respectively, in PADC as a function of the stopping power. The solid square symbols indicate present results for high energy protons and the open symbols show those for previous ones (Mori et al., 2009, 2011). As shown in these figures, the present data lie on the extrapolated lines from 2.7 MeV proton and He ions, indicating greater values at the lower stopping power. Similar dependence on the stopping power for other heavy ions with higher energies was reported in the previous study (Mori et al., 2012). The values for 70 MeV protons are higher than those of gamma ray in the both bonds, which is plotted at 0.2 keV/μm as lateral axis adopting the average linear energy transfer, *LET*, of gamma rays from the Co-60 source. This implies that molecule bond breaking along proton tracks within the single repeat unit suppress the recombination. Each bond breaking due to gamma ray distributes spatially isolated without forming any track structure. This view is also supported by the results that the G values in vacuum are about half for gamma ray and independent for protons (Mori et al., 2013).

Fig. 11. shows the G values for loss of CH groups in PADC for each radiations as a function of the stopping power. The values for 20, 30 and 70 MeV protons are independent to stopping power, different from those of ether and carbonate ester bonds. One can find a clear step between the data of protons and those of heavy ions. As discussion in the previous sections, this step corresponds to the detection threshold for proton (Hassan et al., 2013), that is 17 keV/μm. Among the three chemical damage parameters adopted in the present study, the G value is most suited to point out the clear relation between the track damage structure and the threshold for etchable track formation in PADC.

4.6. Radial dose distribution around the threshold

The radial dose distribution theory has been developed, in which the primary

ionization was taken into account as well as the effects of secondary electrons, and applicable to the polymers as a uniform stopping media (Waligórski et al., 1986). Fig. 12. shows dose distribution around the proton trajectories in PADC with energies of 2.7, 5.7, 20, 30 and 70 MeV. In these calculations, the averaged ionization potential appeared in this theory was treated as a controlling parameter to keep the total deposition energy per unit distance along track to reproduce concordant results with the stopping power given by the SRIM code. The parameter found to be varied between 65 and 120 eV depending on the proton energies. The energy deposition will be done within 800 nm in the case of 2.7 MeV protons, while the maximum distance 300 μm for 70 MeV protons.

The plotted points on each curve are effective track core radius for the loss of ether bond, which is the most radio-sensitive part. Since the largest core radius is 0.5 nm for 2.7 MeV protons, the almost all damage in these proton tracks should be remained within the single repeat unit in the radial direction. We must keep in mind the concept of absorbed dose cannot be easily applied to such small volume, because the media of PADC is never uniform in such scale. The fractions of deposited energy beyond the effective track core radius are 93.0, 94.6, 95.0, 96.5 and 96.0 % for 2.7, 5.7, 20, 30 and 70 MeV protons, respectively. Most of energy deposition occurred out of the effective track core radius. Judging from the high G value for gamma ray, polymeric chains of PADC should be effectively destroyed by secondary electrons not only in track core but also in track hallo or penumbra region. It is hard to make more discussions simply based on the local dose theory and the core radius.

The experimentally confirmed dependence of the G values for the ether and carbonate ester bond on the stopping power indicates that the recombination of broken molecular bonds is effectively suppressed, compared to that for gamma ray (see Figs. 9. and 10.). On the other hand, the G values for loss of CH groups is almost independent to the stopping power and slightly but significantly higher than that of gamma ray (Fig. 11.). The damage along proton tracks with higher energy is similar to that caused by gamma irradiation but never identical. Further studies should be progressed to find chemical damage structure in both sides of the threshold for He and other relatively light ions.

4.7. Dependence of the effective track core radius on the stopping power

The dependence of the effective core radii on the stopping power for losses of ether bonds, carbonate ester bonds and CH groups are shown in Fig. 13., using the obtained experimental formulas expressed as in Eqs. (7), (8), (11), (12), (15) and (16). The core radius of the loss of ether is always largest among the three in the examined region from 1 to 12,000 keV/μm. This means that the ether is the most radio-sensitive

part. There are clear bends on the both fitted line segments for the ether and carbonate ester bonds at about 800 keV/μm. The corresponding core radius is about 2 nm for the loss of ether bonds, which is equivalent to the length of the repeat unit of PADC. The region below 800 keV/μm is called as the first region in which the damage area is limited in one or two repeat units in the radial direction. The region above 800 keV/μm is called as the second region in which two or more than two repeat units are affected in the radial direction. The core radius of CH groups is almost straight between He and Xe ions and has no bend at the boundary of 800 keV/μm. The values are almost equal to that of the carbonate ester bond in the second region but not in the first region. As an exclusive feature, the core radius of CH groups has the gap between the high energy protons and the heavy ions of He and the heavier ions. The gap exists between the two fitted line segments, in which the detection threshold for protons of 17 keV/μm is involved. The core radius is 0.3 nm for the loss of CH groups and the corresponding core radii are 0.78 and 0.42 nm, respectively, for losses of the ether and carbonate ester bonds, respectively. This implies that the breaking of molecule bonds are fairly limited within the single repeat units below the detection threshold.

5. Closing remarks

FT-IR spectral studies have been made for PADC film exposed to 20, 30 and 70 MeV protons, of which energy is significantly higher than the detection threshold. The obtained results were compared to those previously attained for 5.7 MeV proton and heavy ions between He and Xe. It became possible to discuss the chemical damage parameters, namely, damage density, effective track core radius and radiation chemical yield, for loss of ether bonds, carbonate ester bonds and CH groups in the wide range of the stopping power between 1 and 12,000 keV/μm. The chemical damage parameters of the ether and carbonate ester bonds are on the almost identical trends with those of the heavy ions. The size of effective track core of the protons for the loss of CH groups is on the quiet different trend to that of heavy ions and the G values are similar to that of the gamma ray. The graphs of the chemical damage parameters against the stopping power were found to be useful to express the feature of latent tracks.

We are now conducting the further study to examine the track structure around the detection thresholds of protons and He ions in PADC. In addition to this, studies on latent tracks of heavy ions with semi-relativistic energy must be systematically conducted.

Acknowledgments

The authors express our thanks to the NIRS-Cyclotron crew for providing excellent beams.

We also express our thanks to the staff of NIRS-HIMAC for their support during the experiment (H138). This work was made as a part of the Research Project with Heavy Ions at NIRS-HIMAC.

References

Balanzat, E., Betz, N., Bouffard, S., 1995. Swift heavy ion modification of polymers. *Nucl. Instrum. Meth. B.* 105, 46-54.

Barillon, R., Yamauchi, T., 2003. Chemical bond scission induced by $^{1}H^{+}$, $^{16}O^{8+}$, and γ-rays in a cellulose nitrate detector. *Nucl. Instrum. Meth. B.* 208, 336-339.

Barillon, R., Yamauchi, T., Mori, Y., Raffy, Q., 2015. A first attempt to simulate oxidization effects on latent track structure in PADC combining the radial dose theory and a radio-oxidation kinetic model. *Radiat. Meas.* 83, 1-4.

Benton, E.R., Benton, E.V., Frank, A.L., 2002. Passive dosimetry aboard the Mir Orbital Station: internal measurements. *Radiat. Meas*., 35, 439-455.

Cartwright, B.G., Shirk, E.K., Price, P.B., 1978. A nuclear-track-recording polymer of unique sensitivity and resolution. *Nucl. Instrum. Meth. B.* 41, 447-460.

Doke, T., Hayashi, T., Nagaoka, S., Ogura, K., Takeuchi, R., 1995. Estimation of dose equivalent in STS-47 by a combination of TLDs and CR-39. *Radiat. Meas.* 24, 75-82.

Dehaye, F., Balanzat, E., Ferain, E., Legras, R., 2003. Chemical modifications induced in bisphenol A polycarbonate by swift heavy ions. *Nucl. Instrum. Meth. B,* 209, 103-112.

Darraud, C., Bennamane, B., Gagnadre, C., Decossas, J.L., Vareille, J.C., 1993. Optical modifications of polymers by ion beam irradiation. *Polymers* 35, 2447-2451.

Font, L., 2009. On radon surveys: Design and data interpretation. *Radiat. Meas*., 44, 964-968 (2009).

Fukuda, Y., Faenov, A.Ya., Tampo, M., Pikuz, T.A., Nakamura, T., Kando, M., Hayashi, Y., Yogo, A., Sakaki,. H, Kameshima, T., Pirozhkov, A.S., Ogura, K., Mori, M., Esirkepov, T.Zh., Koga, J., Boldarev, A.S., Gasilov, V.A., Magunov, A.I., Yamauchi, T., Kodama, R., Bolton, P.R., Kato, Y., Tajima, T., Daido, H., Bulanov, S.V., 2009. Energy Increase in Multi-MeV Ion Acceleration in the Interaction of a Short Pulse Laser with a Cluster-Gas Target. *Phys. Rev. Lett*., 103, 165002.

Gagnadre, C., Decossas, J.I., Vareille, J.C., 1993. IR spectroscopy studies of polycarbonate irradiated by H^+ and Li^+ ions. *Nucl. Instrum. Meth. B.*, 73, 48-52.

Hassan, N.M., Matai, Y., Kusumoto, T., Mori, Y., Kanasaki, M., Oda, K., Kitamura, H., Konishi, K., Kodaira, S., Yasuda, N., Yamauchi, T., 2013. On the mechanism of the sensitization of PADC (Poly(allyl diglycol carbonate)) track detectors by carbon dioxide treatment. *Radiat. Meas.*, 59, 23-29.

Kanazawa, M., Hojo, S., Sugiura, A., Honma, T., Tashiro, K., Okada, T., Kamiya, T., Takahashi, Y., Suzuki, H., Uchihori, Y., Kitamura, H., 2010. Present operational status of NIRS cyclotrons. In : Proceedings of the 19th International Conference on Cyclotrons and their Applications. Lanzhou, China.

Kodaira, S., Yasuda, N., Konishi, T., Kitamura, H., Kurano, M., Kawashima, H., Uchihori, Y., Ogura, K., Benton, E.R., 2013. Calibration of CR-39 with atomic force microscope for the measurement of short range tracks from proton-induced target fragmentation reactions. *Radiat. Meas*. 50, 232-236.

Kusumoto, T., Mori, Y., Kanasaki, M., Takuya, U., Kameda, Y., Oda, K., Kodaira, K., Kitamura, H., Barillon, R., Yamauchi, T., 2015. Yields on the formation of OH Groups and the loss of CH groups along nuclear tracks in PADC films. *Radiat. Meas.* 83, 59-62.

Lounis-Mokrani, Z., Fromm, M., Barillon, R., Chambaudet, A., Allab, M., 2003. Characterization of chemical and optical modifications induced by 22.5 MeV proton beams in CR-39 detectors. *Radiat. Meas.* 36, 615-620.

Mori, Y., Ikeda, T., Yamauchi, T., Sakamoto, A., Chikada, H., Honda, Y., Oda, K., 2009. Radiation chemical yield for loss of carbonate ester bonds in PADC films exposed to gamma ray. *Radiat. Meas.* 44, 211-213.

Mori, Y., Yamauchi, T., Kanasaki, M., Maeda, Y., Oda, K., Kodaira, S., Konishi, T., Yasuda, N., Barillon, R., 2011. Radiation chemical yields for loss of ether and carbonate ester bonds in PADC films exposed to proton and heavy ion beams. *Radiat. Meas.* 46, 1147-1153.

Mori, Y., Yamauchi, T., Kanasaki, M., Hattori, A., Matai, Y., Matukawa, K., Oda, K., Kodaira, S., Kitamura, H., Konishi, T., Yasuda, N., Tojo, S., Honda, Y., Barillon, R.,2012. Greater radiation chemical yields for lossesof ether and carbonate ester bonds at lower stopping powers along heavy ion tracks in poly(allyl diglycol carbonate) films. *Appl. Phys. Express* 5, 086401.

Mori, Y., Yamauchi, T., Kanasaki, M., Hattori, A., Oda, K., Kodaira, S., Konishi, T., Yasuda, N., Tojo, S., Honda, Y., Barillon, R., 2013. Vacuum effects on the radiation chemical yields in PADC films exposed to gamma rays and heavy ions. *Radiat. Meas.* 50, 97-102.

Nishiuchi, M., Sakaki, H., Esrikepov T.Zh., Nishio, K., Pikuz, T.A., Faenov, A.Ya., Skobelev, I.Yu., Orlandi, R., Sako, H., Pirozhkov, A.S., Matukawa, K., sagisaka, A., Ogura, K., Kanasaki, M., Kiriyama, H., Fukuda, Y., Koura, H., Kando, M., Yamauchi, T., Watanabe, Y., Bulanov, S.V., Kondo, K., Imai, K., Nagamiya, S., 2015. Acceleration of highly-charged GeV Fe ions from a low-Z substrate by intense femtosecond laser. *Phys. Plasmas* 22, 033107.

Oda, K., Imasaka, Y., Yamauchi, T., Nakane, Y., Endo, A., Tawara, H., Yamaguchi, Y., 2005. Radiator design for detecting high-energy neutrons with a nuclear track detector. *Radiat. Meas*. 40, 570-574.

Peterson, F., Enge, W., 1995. Energy loss dependent transversal etching rates of heavy ion tracks in plastic. *Radiat. Meas*. 25, 43-46.

Waligórski, M.P.R., Hamm, R.N., Katz, R., 1986. The radial distribution of dose around the path of a heavy ion in liquid water. *Nucl. Tracks Radiat. Meas.* 11, 309-319.

Yamauchi, T., 2003. Studies on the nuclear tracks in CR-39 plastics. *Radiat. Meas.* 36, 73-81.

Yamauchi, T., Mori, Y., Oda, K., Yasuda, N., Kitamura, H., Barillon, R., 2008a. Structural modification along heavy ion tracks in poly(allyl diglycol carbonate) films. *Jpn. J. Appl. Phys*. 47, 3606-3609.

Yamauchi, T., Watanabe, S., Seto, A., Oda, K., Yasuda, N., Barillon, R., 2008b. Loss of carbonate ester bonds along Fe ion tracks in thin CR-39 films. *Radiat. Meas.* 43, 106-110.

Yamauchi, T., Mori, Y., Oda, K., Kodaira, S., Yasuda, N., Barillon, R., 2010. On the tracks of proton and heavy ions in PC and PADC plastics detectors. In : Proceedings of the 24th Workshop on Radiation Detector and their Uses. KEK Proceedings, Tsukuba, Japan, 10, 1-11.

Yamauchi, T., Mori, Y., Morimoto, A., Kanasaki, M., Oda, K., Kodaira, S., Konishi, T., Yasuda, N., Tojo, S., Honda, Y., Barillon, R., 2012. Thresholds of Etchable Track Formation and Chemical Damage Parameters in Poly(ethylene terephthalate), Bisphenol A polycarbonate, and Poly(allyl diglycol carbonate) Films at the stopping Powers Ranging from 10 to 12,000 keV/μm. *Jpn. J. Appl. Phys.* 51, 056301.

Ziegler, J.F., 2004. SRIM-2003. *Nucl. Instrum. Meth. B.* 219-220, 1027-1036.

Zylstra, A.B., Frenje, J.A., Séguin, F.H., Gatu Johnson, M., Casey, D.T., Rosenberg, M.J., Waugh, C., Sinenian, N., Manuel, M.J.-E., Li, C.K., Petrasso, R.D., Kim, Y., Herrmann, H.M., 2012. A new model to account for track overlap in CR-39 data. *Nucl. Instrum. Meth. A*. 68, 184-90.

Table 1 Removal cross sections of ether, carbonate ester and CH groups for high energy protons and Ne ions

	Proton			Ne
Energy (MeV)	20	30	70	83
Stopping power (keV/μm)	3.6	2.5	1.2	1100
σ_{Ether} (cm^2)	$(3.22\pm1.02)\times10^{-15}$	$(2.10\pm0.15)\times10^{-15}$	$(1.89\pm0.10)\times10^{-15}$	$(2.14\pm0.20)\times10^{-13}$
$\sigma_{C=O}$ (cm^2)	$(1.58\pm0.36)\times10^{-15}$	$(0.92\pm0.25)\times10^{-15}$	$(0.62\pm0.10)\times10^{-15}$	$(1.16\pm0.15)\times10^{-13}$
σ_{CH} (cm^2)	$(1.52\pm0.87)\times10^{-15}$	$(0.81\pm0.30)\times10^{-15}$	$(0.44\pm0.08)\times10^{-15}$	$(1.13\pm0.09)\times10^{-13}$

Figure Captions

Fig. 1. A repeat unit of PADC.

Fig. 2. Reduction of the relative absorbance of ether bond, carbonate ester bond and CH groups in PADC exposed to 70 MeV protons. The slope of each fitted line corresponds to the removal cross section.

Fig. 3. Damage density for the loss of ether bond against the stopping power, solid square symbols are present work, open symbols are previous ones (Mori et al., 2011, 2012). The first region and the second one are separated at the stopping power of 800 keV/μm.

Fig. 4. Effective track core radius for loss of ether bond as a function of the stopping power, solid square symbols are present work, open symbols are previous ones (Mori et al., 2011, 2012). The effective track core radius is about 2 nm at the boundary of the two regions.

Fig. 5. Damage density for the loss of carbonate ester bond against the stopping power, solid square symbols are present work, open symbols are previous ones (Mori et al., 2011, 2012). The first region and the second one are separated at the stopping power of 800 keV/μm.

Fig. 6. Effective track core radius for loss of carbonate ester bond as a function of the stopping power, solid square symbols are present work, open symbols are previous ones (Mori et al., 2011, 2012). The effective track core radius is about 1.2 nm at the boundary of the two regions.

Fig. 7. Damage density for the loss of CH groups against the stopping power. The indicating arrow is the detection threshold of protons.

Fig. 8. Effective track core radius for loss of CH groups as a function of the stopping power, solid square symbols are present work, open symbols are previous ones (Kusumoto et al., 2015). The indicating arrow is the detection threshold of protons.

Fig. 9. G value for loss of ether bond as a function of the stopping power, solid square

symbols are present work, open symbols are previous ones (Mori et al., 2011, 2012). The broken line is for eye guide.

Fig. 10. G value for loss of carbonate ester bond as a function of the stopping power, solid square symbols are present work, open symbols are previous ones (Mori et al., 2011, 2012). The broken line is for eye guide.

Fig. 11. G value for loss of CH groups as a function of the stopping power. The broken line is for eye guide.

Fig. 12. Radial dose distributions around the ion path of 2.7, 5.7, 20, 30 and 70 MeV protons in PADC. The ionizing potential is treated as a controlling parameter to reproduce the identical stopping power to that from the SRIM code.

Fig. 13. Effective track core radius for losses of ether bond, carbonate ester bond and CH groups. The modified structure along the tracks in PADC are divided in the three phases for the protons and the heavy ions with energies less than 6 MeV/n.

Fig. 1. Kusumoto et al., 2015

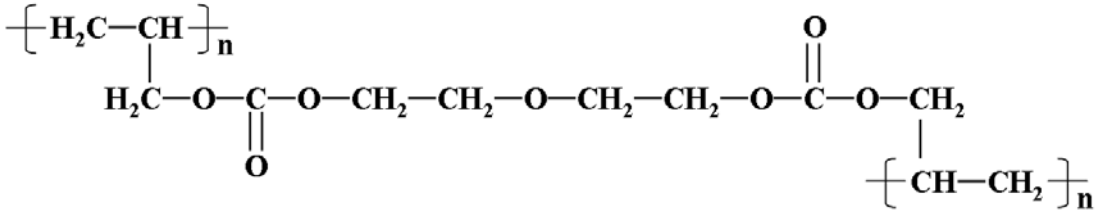

Fig. 2. Kusumoto et al., 2015

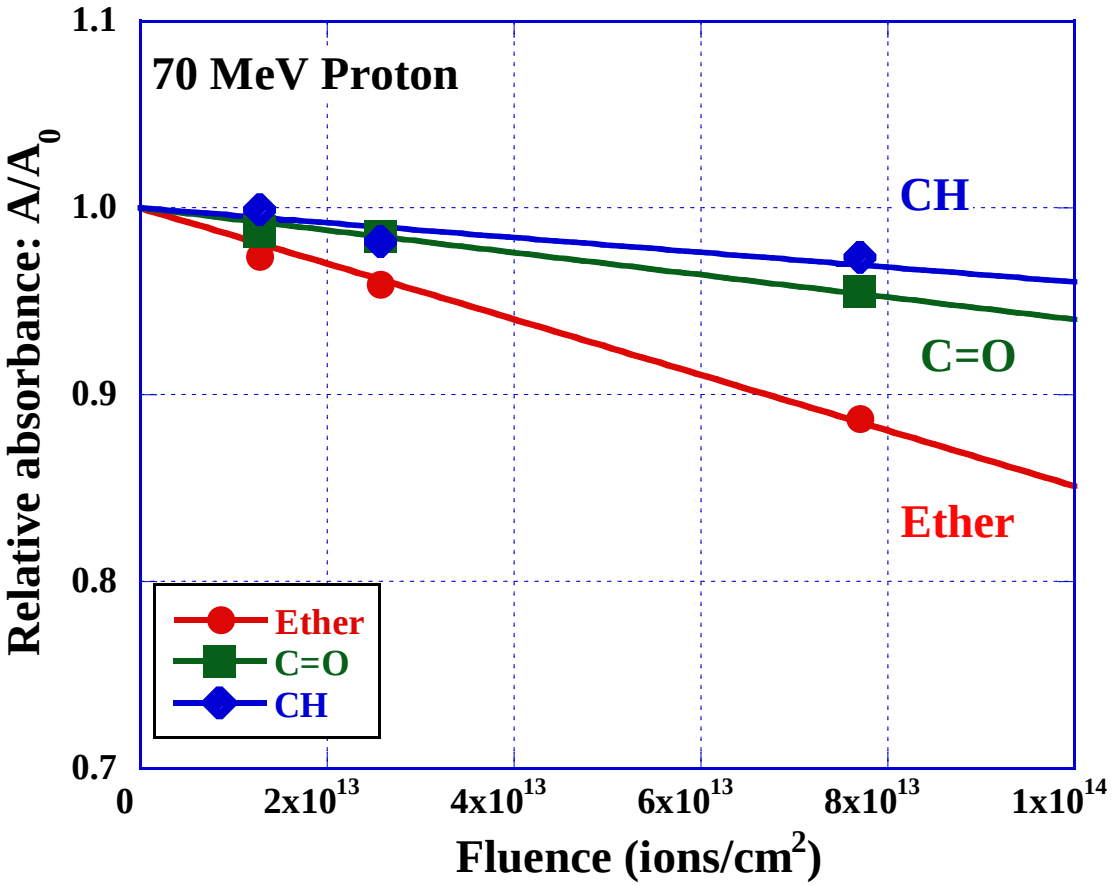

Fig. 3. Kusumoto et al., 2015

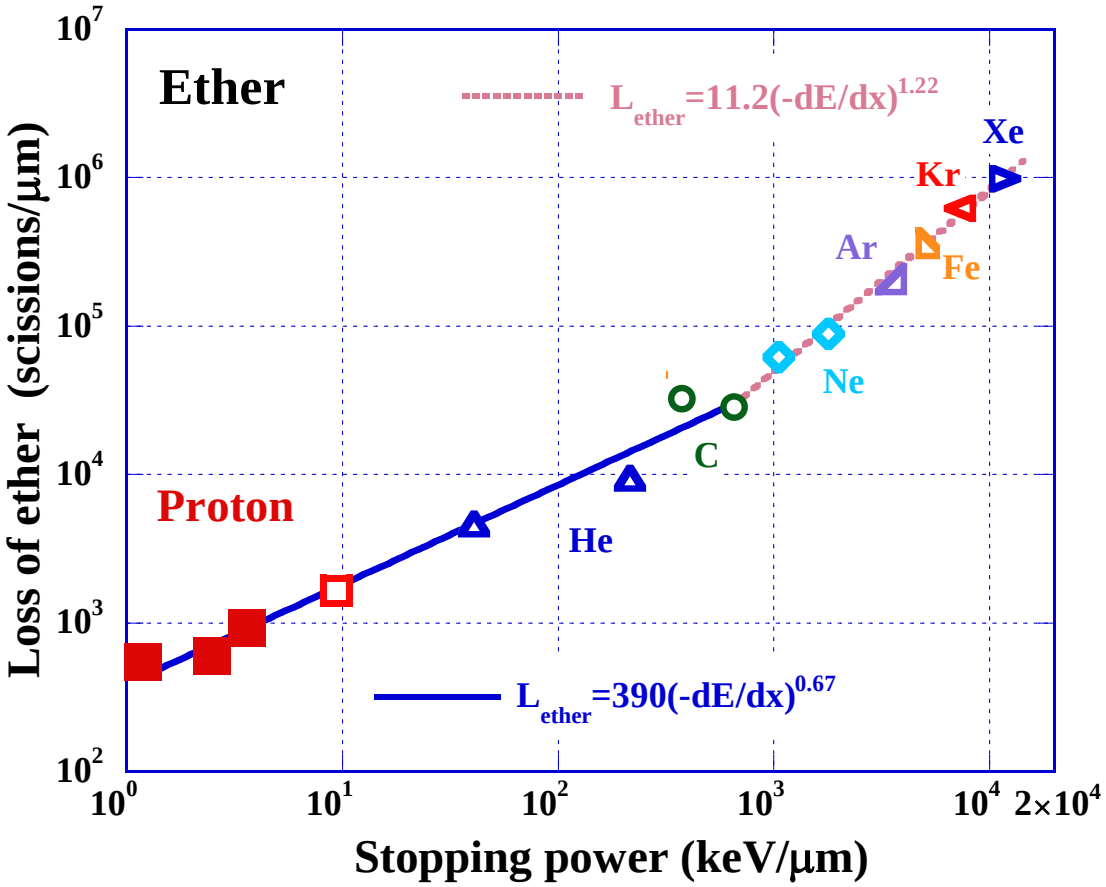

Fig. 4. Kusumoto et al., 2015

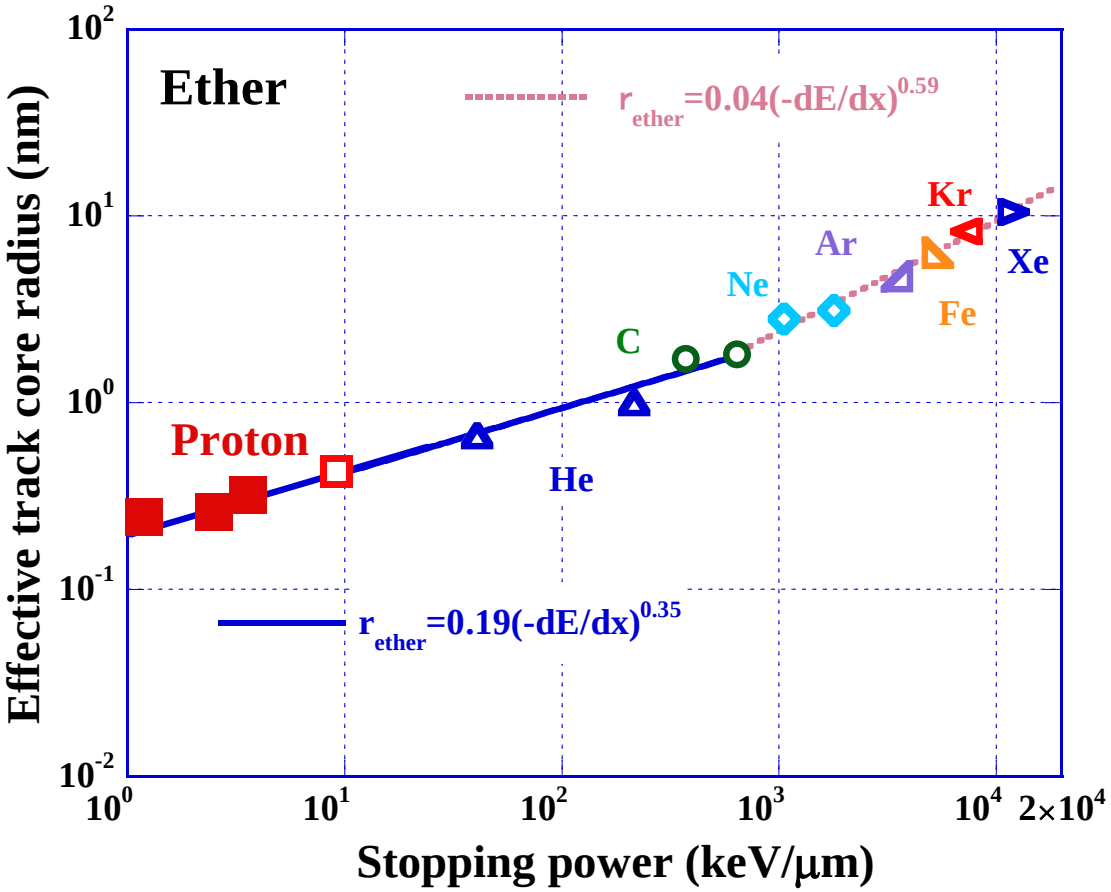

Fig. 5. Kusumoto et al., 2015

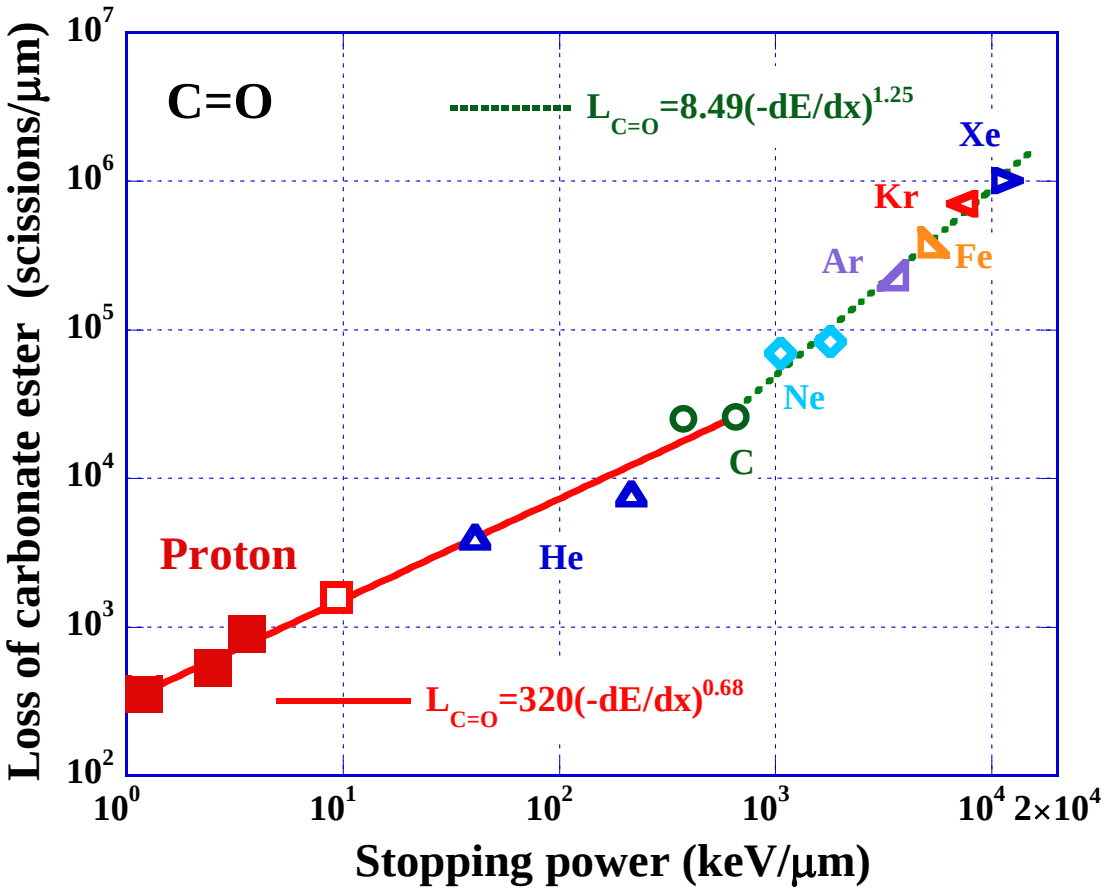

Fig. 6. Kusumoto et al., 2015

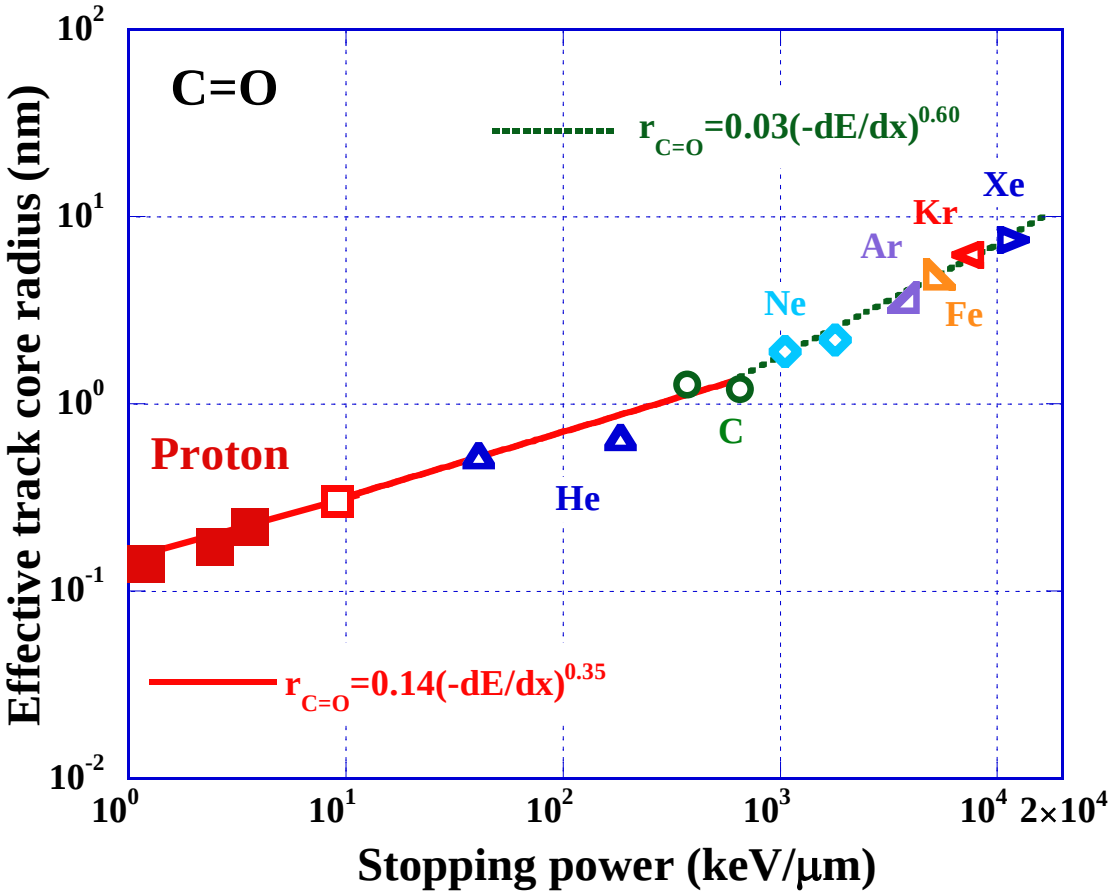

Fig. 7. Kusumoto et al., 2015

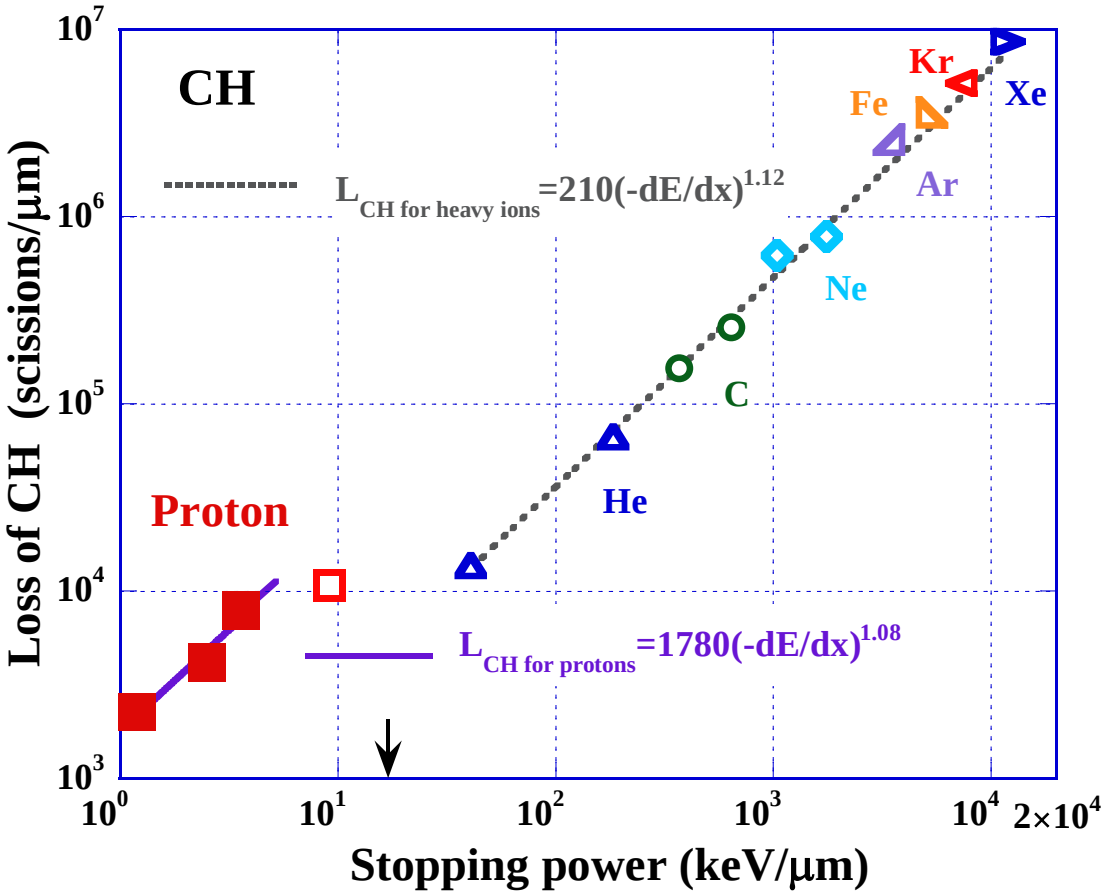

Fig. 8. Kusumoto et al., 2015

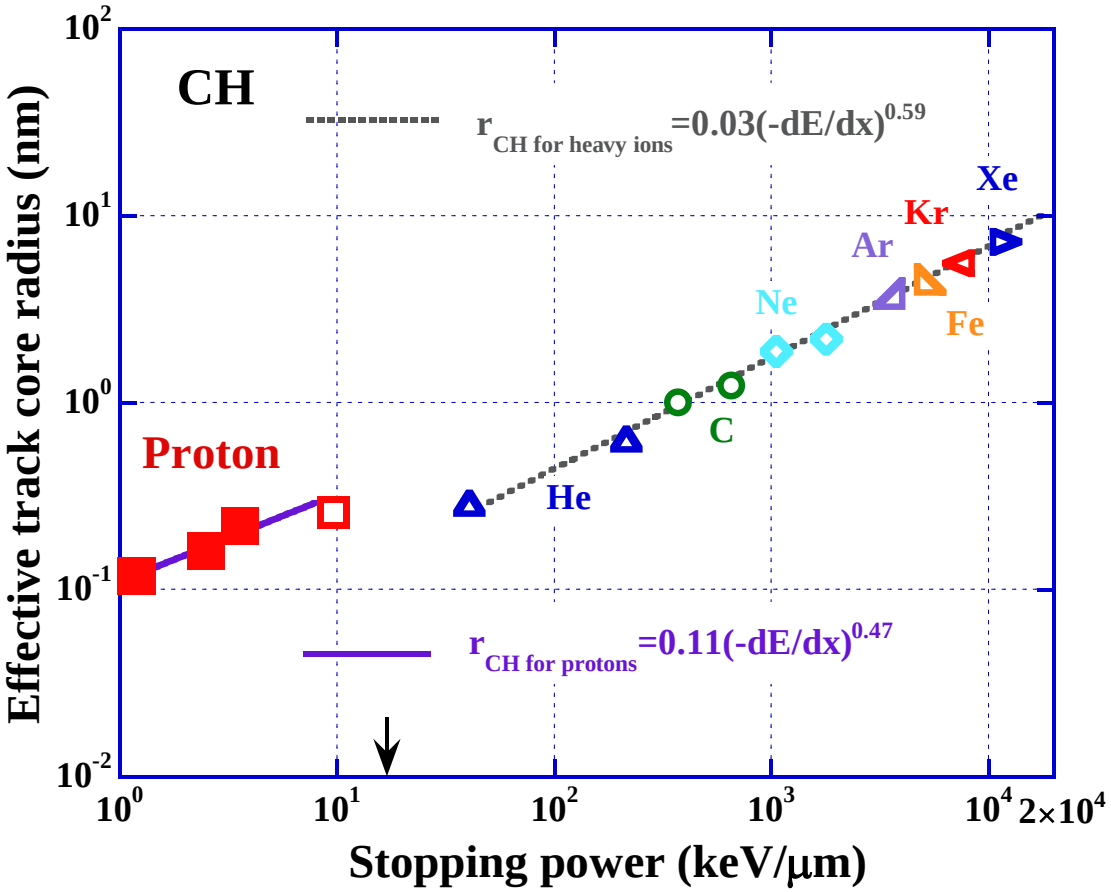

Fig. 9. Kusumoto et al., 2015

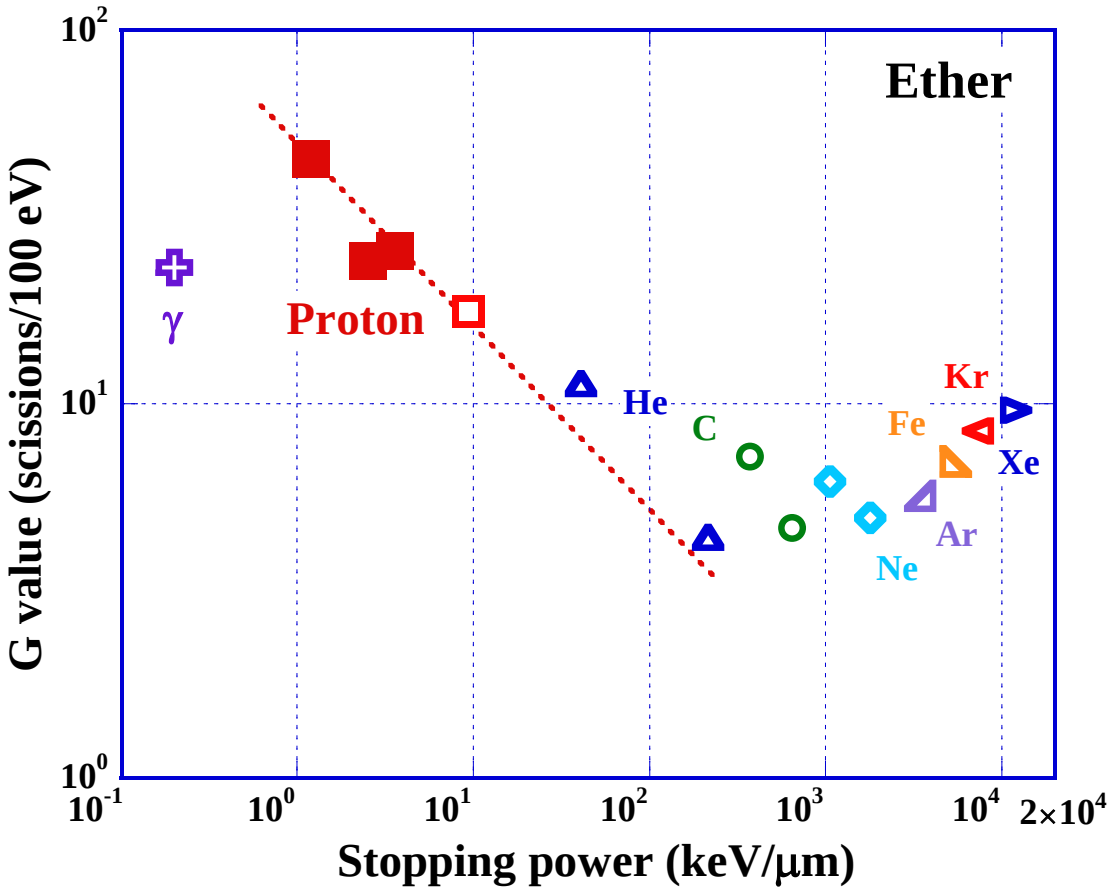

Fig. 10. Kusumoto et al., 2015

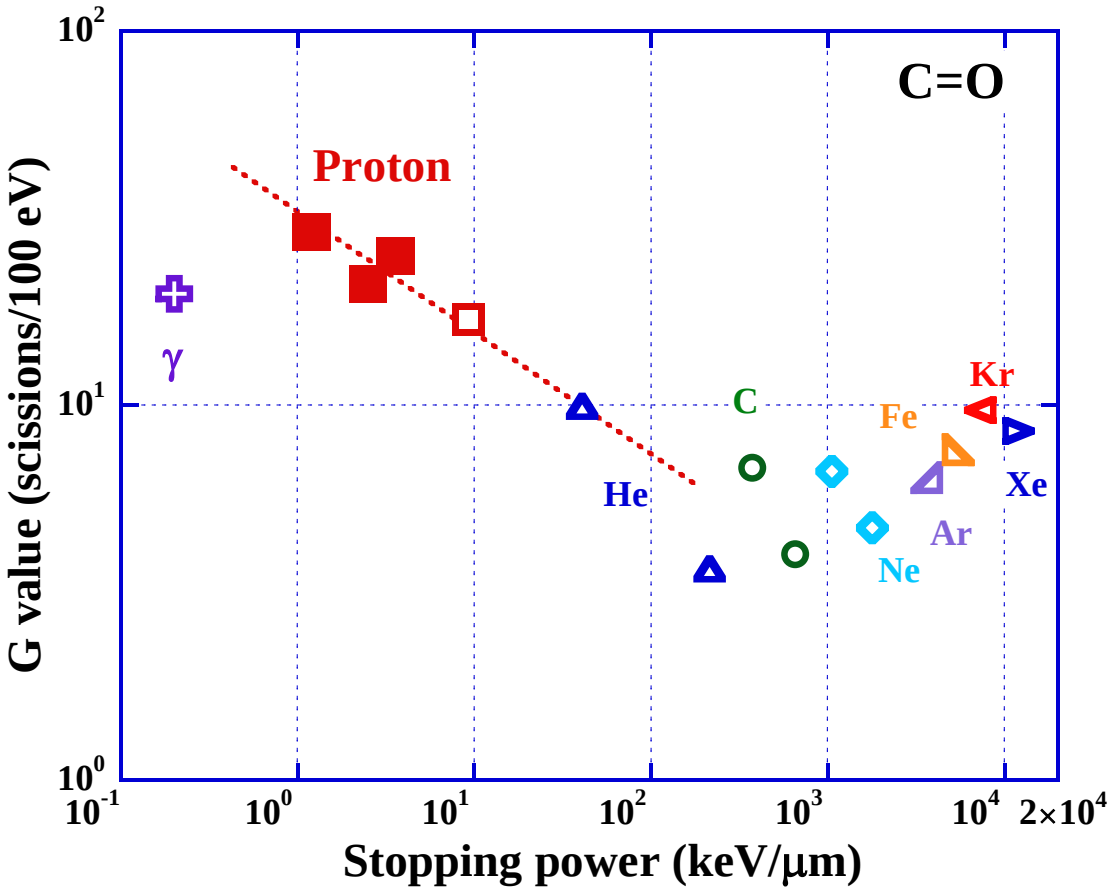

Fig. 11. Kusumoto et al., 2015

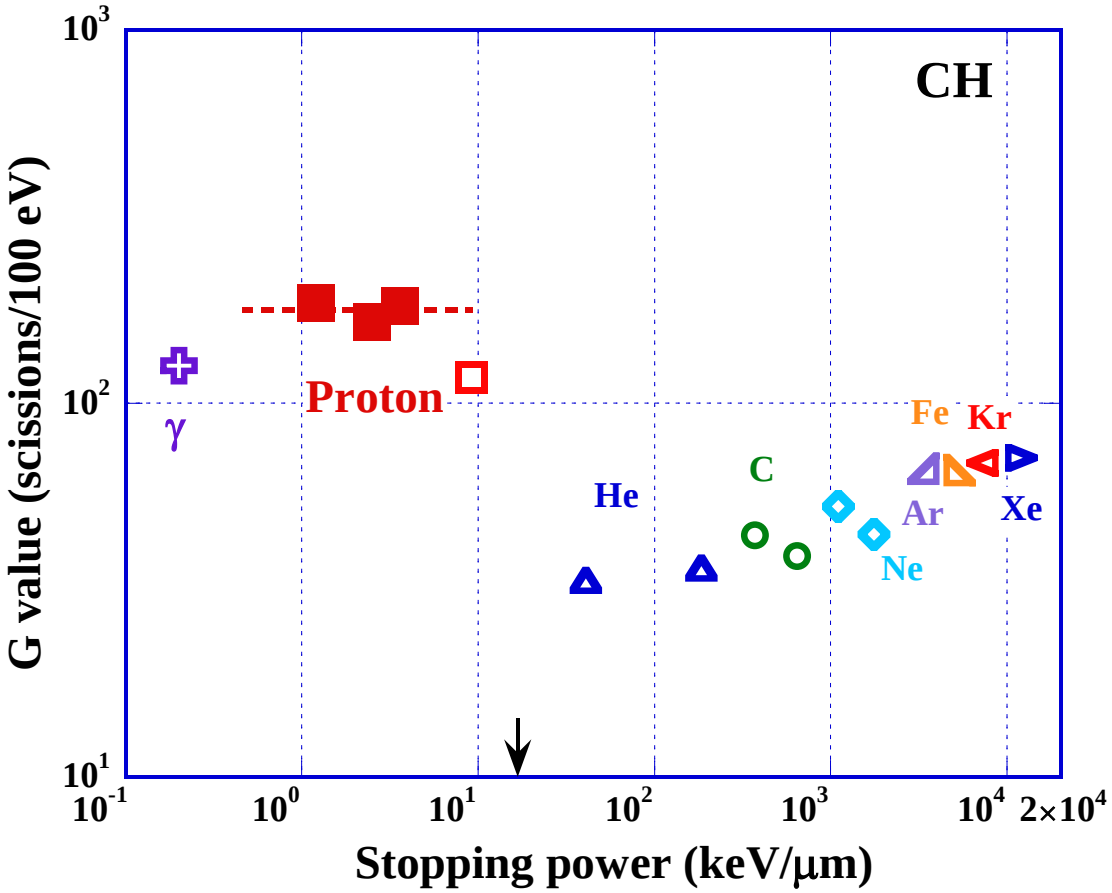

Fig. 12. Kusumoto et al., 2015

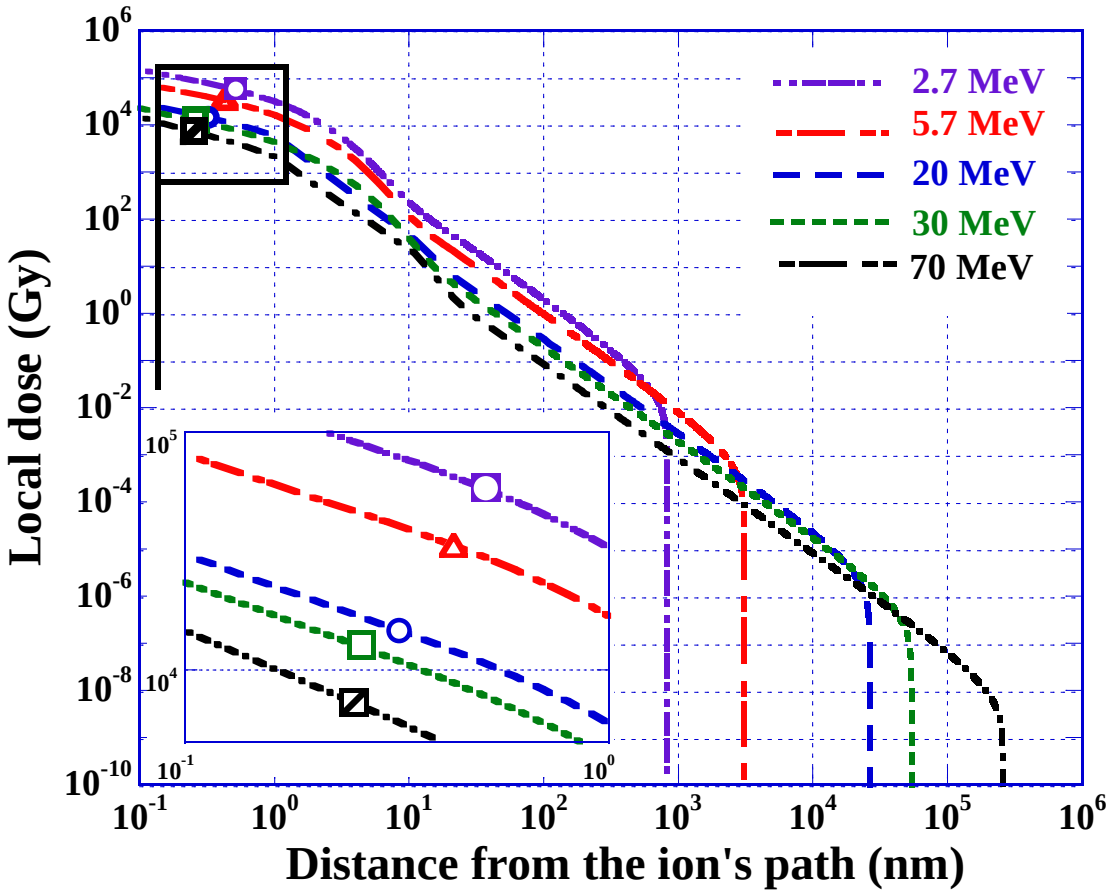

Fig. 13. Kusumoto et al., 2015